Composites: Part B 59 (2014) 173–180

Contents lists available at ScienceDirect

Composites: Part B

journal homepage: www.elsevier.com/locate/compositesb

Modeling of soft composites under three-dimensional loading

F. López Jiménez *

Laboratoire de Mécanique des Solides, UMR CNRS 7649, École Polytechnique, 91128 Palaiseau Cedex, France

ARTICLE INFO

Article history:
Received 21 June 2013
Received in revised form 19 September 2013
Accepted 12 November 2013
Available online 25 November 2013

Keywords:
A. Fibers
B. Mechanical properties
C. Finite element analysis (FEA)

ABSTRACT

The finite deformation response of fiber-reinforced hyperelastic solids under three-dimensional loading is studied through finite element simulations. The composites are modeled using representative volume elements with random fiber arrangement and periodic boundary conditions. Different matrices and volume fractions are considered. It is found that the shear stiffness of composites with Neo-Hookean components depends on the direction of the applied deformation even when the fibers are not stretched, which indicates a clear dependance on not only the $\bar{I}_1$ and $\bar{I}_4$ invariants, but also on $\bar{I}_5$. This anisotropy increases with the fiber concentration. The effect of using an Ogden matrix with increased nonlinearity is also discussed. Finally, the simulations are compared with suitable homogenization techniques available in the literature. A prediction using two different values of the shear stiffness is able to accurately model the response regardless of the loading direction.

1. Introduction

Soft solids reinforced with significantly stiffer fibers are used in technological applications (car tires, carbon fiber-reinforced elastomers) and can also be found in biological tissue (cornea, arterial walls). The difference in stiffness between the two components can reach several orders of magnitude, which leads to micromechanics not observed in traditional fiber composites, such as significant changes in the fiber orientation.

Phenomenological models for the large deformation of fiber reinforced solids usually follow the framework of Spencer [24], considering a homogeneous solid whose strain energy density $\widetilde{W}$ is the sum of two terms:

$$\widetilde{W}(\bar{I}_1,\bar{I}_2,\bar{I}_3,\bar{I}_4,\bar{I}_5) = \widetilde{W}_{iso}(\bar{I}_1,\bar{I}_2,\bar{I}_3) + \widetilde{W}_{aniso}(\bar{I}_4,\bar{I}_5) \quad (1)$$

where the first term represents an isotropic material, and the second term takes into account the anisotropy introduced by the presence of the fiber reinforcements. The invariants $\bar{I}_1$ to $\bar{I}_3$ are the invariants of the average Cauchy-Green deformation gradient $\overline{\mathbf{C}} = \overline{\mathbf{F}}^{\mathrm{T}}\overline{\mathbf{F}}$. These three invariants are isotropic, as opposed to the fourth and fifth: $\bar{I}_4 = \mathbf{N}^{\mathrm{T}}\overline{\mathbf{C}}\mathbf{N}$ measures the stretch in the fiber direction, defined by the vector $\mathbf{N}$, while $\bar{I}_5 = \mathbf{N}^{\mathrm{T}}\overline{\mathbf{C}}\overline{\mathbf{C}}\mathbf{N}$ depends on the fiber stretch and shear and has no straightforward physical interpretation. In most models each term in Eq. (1) depends on a single invariant, $\widetilde{W}_{iso} = \widetilde{W}_{iso}(\bar{I}_1)$ and $\widetilde{W}_{aniso} = \widetilde{W}_{aniso}(\bar{I}_4)$.

Determining the function $\widetilde{W}$ for matrix-dominated deformations is particularly difficult. It is not equal to the strain energy density of the bulk matrix under the same macroscopic deformation, since it needs to take into account the effect of the inclusions, ranging from stress concentrations to possible changes in microstructure as a result of finite deformations. This is sometimes achieved by fitting experimental results under different loading conditions to the force–displacement relationships obtained from Eq. (1) [20,21]. When the experimental data available is not sufficient, as in the case of fiber reinforced elastomers, models found in the literature often use simple geometrical approximations based on periodic microstructures [5,8].

Estimates for the in-plane response of hyperelastic fiber-reinforced solids with particular microstructures using the second-order homogenization scheme have been presented by Ponte Castañeda and co-workers [16,1]. deBotton [3,4] produced estimates for sequentially-coated composites, obtained by successive lamination of the previous composite with thin layers of the matrix phase. These analytical predictions have been compared with finite element simulations [18] with good agreement up to moderate values of the volume fraction. Lopez-Pamies and Idiart [15] have recently proposed an iterative homogenization technique and used it to produce estimates for the three-dimensional response of fiber reinforced elastomers with a random distribution of parallel fibers. This is particularly interesting to model the in-plane buckling of such composites under bending [11,9], since such instabilities result in complex three-dimensional deformation of the material. The applicability of these predictions to three-dimensional loading has not yet been contrasted numerically or experimentally.

This paper presents a series of numerical simulations in two-dimensional and three-dimensional representative volume elements (RVEs) of fiber-reinforced elastomers, with different fiber

* Tel.: +33 686178830.
E-mail address: lopez@lms.polytechnique.fr

1359-8368/$ - see front matter © 2013 Elsevier Ltd. All rights reserved.
http://dx.doi.org/10.1016/j.compositesb.2013.11.020

volume fractions and loading directions. The results are compared to current homogenization models, whose hypothesis and range of validity are discussed. In particular, it will be shown that the shear stiffness of the composite depends on the loading direction, even within the linear regime.

2. Computational model

The composite is idealized as a soft hyperelastic solid reinforced with perfectly parallel cylindrical fibers several orders of magnitude stiffer than the matrix. All the fibers have the same radius r. The fiber volume fraction is V_f, and four values ranging from 0.2 to 0.5 are considered. It is assumed that no voids exist in the composite, and bonding between fibers and matrix is perfect. The strain softening reported by López Jiménez and Pellegrino [11] is therefore neglected here.

A series of 2D and 3D finite element simulations on representative volume elements (RVEs) have been performed using the commercial package Abaqus. Schematics of the geometry and reference systems for the models are shown in Fig. 1. The RVEs are square in the plane perpendicular to the fiber direction, $L_2 = L_3 = L$, and have length L_1 along the fiber direction.

The following subsections give details on the model, such as material properties used for each component, fiber arrangement, size of the RVE and boundary conditions.

2.1. Material properties

The fibers are modeled as a Neo-Hookean material with elastic shear modulus μ_f. The Poisson's ratio is taken as $\nu_f = 0.3$, although the simulations show that the fibers behave as a rigid body, and so the results are insensitive to the value of ν_f. The matrix has been modeled as an incompressible Ogden hyperelastic solid [19], in which the strain energy W_m takes the form:

$$W_m = \sum_{i=1}^{N} \frac{2\mu_i}{\alpha_i^2}\left(\lambda_1^{\alpha_i} + \lambda_2^{\alpha_i} + \lambda_3^{\alpha_i} - 3\right) \tag{2}$$

In order to check the effect of the large strain behavior of the matrix, three different combinations of N and α_i have been considered. The first one, $N = 1$ and $\alpha = 2$, corresponds to a Neo-Hookean material. The other two are respectively softer and stiffer at large elongations; the values are shown in Table 1, and the response of all three matrices to uniaxial tension is shown in Fig. 2. The elastic shear modulus is $\mu_m = \sum_{i=1}^{N} \mu_i$. It is assumed that $\mu_m \ll \mu_f$, which is the case of typical elastomers reinforced with materials such as steel or carbon fibers, as well as several biological tissues. In this case, the results can be scaled by μ_m, see Section 4.1.

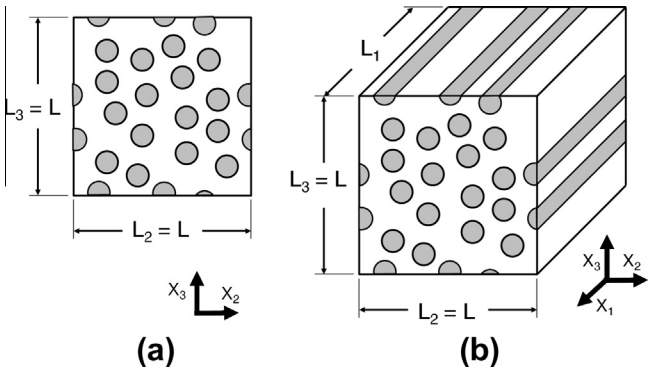

Fig. 1. Representative volume elements (RVEs) used in: (a) two-dimensional and (b) three-dimensional simulations.

Table 1
Parameters of the Ogden hyperelastic energy functions.

	Matrix 1	Matrix 2	Matrix 3
α_1	2	1.2	2.5
μ_1/μ_m	1	0.8	1.01
α_2	0	1	5
μ_2/μ_m	0	0.2	0.02
α_3	0	0	−1
μ_3/μ_m	0	0	−1

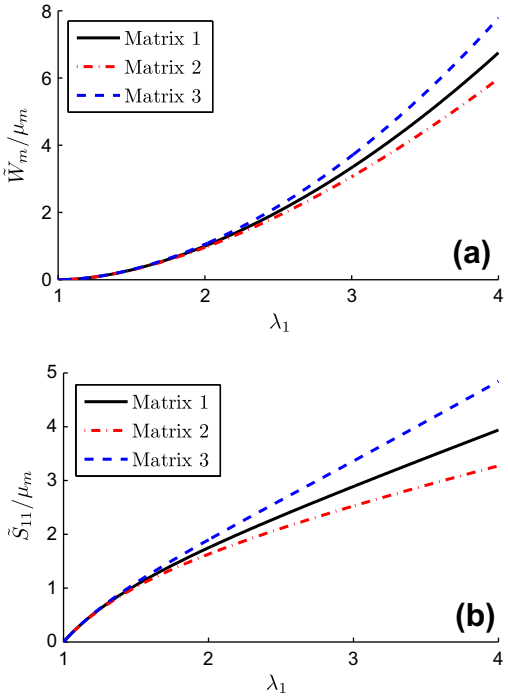

Fig. 2. Response of the three matrices to uniaxial tension: (a) strain energy density normalized by the initial shear stiffness vs. elongation and (b) nominal stress normalized by initial shear stiffness vs. elongation.

2.2. Boundary conditions and applied loading

Periodic boundary conditions are applied in all faces of the RVE using the command `EQUATION` in Abaqus. This requires the mesh to be identical in all opposite faces of the RVE. The conditions can be summarized as:

$$\begin{aligned} \mathbf{u}(L_1, X_2, X_3) - \mathbf{u}(0, X_2, X_3) &= \overset{1}{\mathbf{u}} \\ \mathbf{u}(X_1, L_2, X_3) - \mathbf{u}(X_1, 0, X_3) &= \overset{2}{\mathbf{u}} \\ \mathbf{u}(X_1, X_2, L_3) - \mathbf{u}(X_1, X_2, 0) &= \overset{3}{\mathbf{u}} \end{aligned} \tag{3}$$

where $\overset{i}{u}_j = \bar{F}_{ij} L_j$, L_j is the length of the RVE in the jth direction, and $\bar{\mathbf{F}}$ is the applied deformation gradient, $\bar{F}_{ij} = \partial x_i / \partial X_j$.

The components of $\overset{i}{\mathbf{u}}$ are the displacements of auxiliary dummy nodes, in which displacement or loadings can be imposed. Due to the high difference in stiffness between fibers and matrix, the response of the composite is dominated by the fiber behavior for any deformation involving stretching of the fibers, $\bar{I}_4 \neq 1$. Since the goal is to study the dependance on other invariants, loading will be limited to cases in which no stretching is imposed on the fibers.

2.3. Model size

The number of fibers in the RVE must be sufficient to ensure that the mechanical properties predicted by the model do not depend on the particular fiber arrangement, and are therefore representative of the limit case of an infinite composite. In addition, nonlinear elasticity requires larger RVE sizes than the linear case. Khisaeva and Ostoja-Starzewski [7] performed numerical studies showing very good approximations for a RVE size of $L/d = 16$, where d is the fiber diameter and $L = L_2 = L_3$. These results were later confirmed in by Moraleda et al. [18], and are therefore used here. Table 2 shows the number of fibers and RVE size as a function of the fiber volume fraction.

Regarding the out of plane direction, the simulations show that due to the periodic boundary conditions all microscopic fields are invariant with respect to the X_3 coordinate, even for three-dimensional loading. The value of L_3 is therefore arbitrary, and no difference in the results can be observed once the models have more than four elements in the X_3 direction.

In all cases it is implicitly assumed that the composite will remain in its principal solution under the applied loading. If instabilities were induced, then the response of the model would strongly depend on the ratio between its size and the instability wavelengths [17,2,23].

2.4. Fiber arrangement

Since the composite is idealized as having perfectly parallel fibers, their arrangement is fully described by the position of the centers in a square, two-dimensional RVE. They are initially distributed following a hard-core process. This is a Poisson process in which a limitation on the minimum distance between the centers is introduced: the positions are obtained randomly, and rejected if the distance to any of the already allocated fibers is less than a given limit. In this work, the minimum distance adopted is 1.1 times the diameter. Additionally, a fiber is also rejected if the distance between its center to the edge of the RVE is in the $[0.9r, 1.1r]$ interval. The goal of both conditions is creating a geometry that can be easily meshed.

High volume fractions might reach the jamming limit, given by Tanemura [25] as 0.547 and further lowered by the imposed additional restrictions. If after 1000 attempts a new fiber has not been accepted, the last attempted position is accepted even if it overlaps with other fibers. In such cases the Random Sequential Adsorption [22] algorithm is used. It is an iterative process that tries to minimize a potential E, which in this case is defined as:

$$E = \sum_i \sum_j \delta_{ij}\left(10 + \frac{100r}{d_{ij}}\right) + 100\sum_i \delta_i \tag{4}$$

where d_{ij} is the distance between the ith and jth fibers, and δ_{ij} and δ_i are equal to one if the restrictions to the location of the fibers are not satisfied by the ith and jth fibers, or by the ith fiber and the edges of the RVE, respectively.

Once this potential is defined, the algorithm works as follows: In every iteration a fiber is picked randomly, and a small random displacement is assigned. The potential E' is calculated for this new configuration. The displacement is accepted according to the probability:

$$P = \begin{cases} 1 & \text{if } \Delta E \leqslant 0 \\ e^{\frac{E-E'}{A}} & \text{if } \Delta E > 0 \end{cases} \tag{5}$$

where $\Delta E = E' - E$ and A is a parameter that controls how fast the system evolves. This means that the algorithm would accept some of the displacements in which the energy increases slightly, but almost none producing a large increment. The iterations are repeated until the energy of the system reaches $E = 0$, corresponding to a configuration where all restrictions are satisfied. Examples of the fiber arrangements obtained for $V_f = 0.2$ and $V_f = 0.5$ are shown in Fig. 3.

Table 2
Number of fibers and value of L/r for the four fiber volume fractions V_f considered.

V_f	0.2	0.3	0.4	0.5
Number of fibers	65	100	130	160
L/d	15.98	16.18	15.98	15.85

2.5. Mesh

The two-dimensional fiber arrangement is meshed with a combination of triangle elements in the fibers and rectangular quadrilateral elements in the matrix. This mesh is then transported in the fiber direction, producing a three-dimensional mesh consisting of triangular and rectangular prisms.

Regarding the type of elements, the fibers are modeled using linear triangular elements for plane strain (CPE3) in 2D models or triangular prisms (C3D6) in 3D models. Since the matrix is modeled as an incompressible material, it requires the use of elements with hybrid formulation. Linear quadrilateral elements produced the same results as second order triangular elements with better convergence, and so CPE4H are used in 2D simulations and C3D8H for 3D cases.

A parametric study of the mesh size produced different results for each type of RVE considered. In the two-dimensional simulations, the applied loading leads to significant changes in the relative position of the fibers, and a very fine mesh is required to achieve convergence. As a rough estimate, at least four matrix elements are needed between the closest fibers. An average element size of $0.05r$ has been chosen, producing models with 415 000–480 000 elements and 320 000–445 000 nodes.

In the three-dimensional loadings the mesh is not as fine, in order to reduce the computational cost. The models in this study have an average element size of $0.075r$ and four elements in the X_1 direction, resulting in models with 730 000–850 000 elements and 720 000–980 000 nodes.

3. Homogenization based models

This section presents a brief summary of basic notation in homogenization theory, as well as the main results from the works used for comparison with the simulations. A complete review of homogenization is beyond the scope of this work. The reader is referred to the articles referenced here and in Section 1.

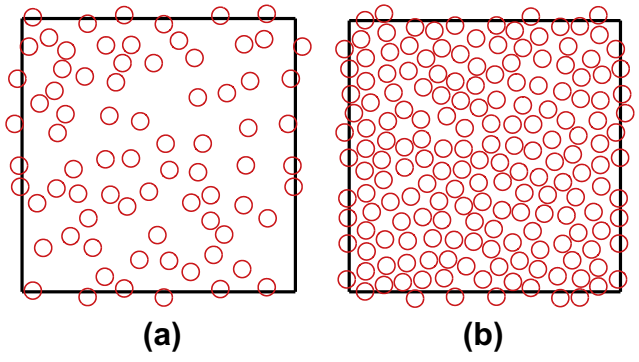

Fig. 3. Fiber arrangement of RVEs with: (a) $V_f = 0.2$ and (b) $V_f = 0.5$.

The macroscopic response of a fiber-reinforced material is usually described by the relation between its average stress $\overline{\mathbf{S}}$ and the average deformation gradient $\overline{\mathbf{F}}$ [6]:

$$\overline{\mathbf{S}} = \frac{\partial \overline{W}}{\partial \overline{\mathbf{F}}} \tag{6}$$

Here, the effective stored-energy function $\overline{W}$ is defined as:

$$\overline{W}(\overline{\mathbf{F}}) = \min_{\mathbf{F}\in K(\overline{\mathbf{F}})} \frac{1}{V}\int_V W(\mathbf{F},\mathbf{X})d\mathbf{X} \tag{7}$$

where V is the volume of the composite, and $K(\overline{\mathbf{F}})$ is the set of admissible deformation gradients $\mathbf{F}$ consistent with the average condition:

$$\overline{\mathbf{F}} = \frac{1}{V}\int_V \mathbf{F}(\mathbf{X})d\mathbf{X} \tag{8}$$

Homogenization techniques aim to provide the strain energy density $\widetilde{W}(\overline{\mathbf{F}})$ of a homogeneous solid that servers as an estimate for the effective stored-energy function $\overline{W}$ of a composite, as a function of its microstructure and the material properties of its components.

deBotton et al. [3,4] and Lopez-Pamies and Idiart [15] have made use of iterative techniques based on solutions for coated laminates. The corresponding estimate of the real material strain energy, $\widetilde{W}_{SCC}$, is an exact solution for the assumed composite geometry. The result reads as follows:

$$\widetilde{W}_{SCC} = \tilde{\mu}_{HS}(\bar{I}_1 - 3) + \frac{\tilde{\mu}_n - \tilde{\mu}_{HS}}{2}\frac{\left(\sqrt{\bar{I}_4}+2\right)\left(\sqrt{\bar{I}_4}-1\right)^2}{\sqrt{\bar{I}_4}} \tag{9}$$

where $\tilde{\mu}_n$ is the stiffness of the fiber-dominated response:

$$\tilde{\mu}_n = (1-V_f)\mu_m + V_f\mu_f \tag{10}$$

and the linear shear stiffness $\tilde{\mu}_{HS}$ coincides with the Hashin–Shtrikman (H–S) lower bound for the initial shear moduli of transversely isotropic materials with incompressible components:

$$\tilde{\mu}_{HS} = \frac{(1-V_f)\mu_m + (1+V_f)\mu_f}{(1+V_f)\mu_m + (1-V_f)\mu_f}\mu_m \tag{11}$$

If the fibers are not stretched, $\bar{I}_4 = 1$, Eq. (9) depends only on $\bar{I}_1$, which means that the shear stiffness of the composite, $\tilde{\mu}_{HS}$, does not depend on the loading direction.

The solution in Eq. (9) can be utilized within the iterated homogenization framework [14] to generate in turn a solution for fiber-reinforced Neo-Hookean materials with fibers of circular cross section and polydisperse sizes, i.e. of infinitely many diameters. The resulting effective stored-energy function depends on $\bar{I}_1, \bar{I}_4$ and $\bar{I}_5$, and reads as follows [13]:

$$\widetilde{W}_{IH} = \frac{\tilde{\mu}_{IH}}{2}(\bar{I}_1 - 3) + \frac{\tilde{\mu}_n - \tilde{\mu}_{IH}}{2}\left(\frac{2}{\sqrt{\bar{I}_4}} - 3\right) + \frac{\tilde{\mu}_n - \tilde{\mu}_{HS}}{2}\bar{I}_4 - \frac{\tilde{\mu}_{IH} - \tilde{\mu}_{HS}}{2}\frac{\bar{I}_5}{\bar{I}_4} \tag{12}$$

where

$$\tilde{\mu}_{IH} = (1-V_f)^2\left(1 + \frac{2(2-V_f)V_f}{(1-V_f)^2}\frac{\mu_f}{\mu_m} + \frac{\mu_f^2}{\mu_m^2}\right)\frac{\mu_m}{2} - (1-V_f)^2 \times \sqrt{\frac{2}{(1-V_f)^2}\frac{\mu_f}{\mu_m} + \left(1 + \frac{2(2-V_f)V_f}{(1-V_f)^2}\frac{\mu_f}{\mu_m} + \frac{\mu_f^2}{\mu_m^2}\right)} \times \frac{\mu_f - m u_m}{2} \tag{13}$$

If the fibers are not stretched, Eq. (12) reduces to:

$$\widetilde{W}_{IH}(\bar{I}_4 = 1) = \frac{\tilde{\mu}_{IH}}{2}(\bar{I}_1 - 3) - \frac{\tilde{\mu}_{IH} - \tilde{\mu}_{HS}}{2}(\bar{I}_5 - 1) \tag{14}$$

Due to the dependance on I_5 the material exhibits different behavior depending on the loading direction. In particular, the stiffness for in-plane shear (shear in the $X_2 - X_3$ shear) is $\tilde{\mu}_{IH}$, while for out-of-plane shear (planes $X_1 - X_2$ and $X_1 - X_3$) it is equal to $\tilde{\mu}_{HS}$.

4. Results

As explained in Section 2.2, this study focuses on cases in which the fibers are not stretched, $\bar{I}_4 = 1$. The simulations show that in that case the strain energy in the matrix is orders of magnitude higher than the strain energy in the fibers.

All loadings are characterized by the macroscopic applied average deformation gradient, $\overline{\mathbf{F}}$, or the corresponding principal stretches and invariants. The results are presented normalized by either the initial shear stiffness of the matrix, μ_m, or by the strain energy density of the matrix material under the same macroscopic deformation, W_m. Two main cases are considered: shear in the $X_2 - X_3$ plane (in-plane shear, for which the two-dimensional RVEs are used) and shear in the $X_1 - X_3$ plane (out-of-plane shear), plus combinations of the two.

4.1. In-plane shear

Due to the high fiber stiffness and the incompressibility of the elastomeric matrix, the composite can be approximated as an incompressible solid. Stretching and shearing in the $X_2 - X_3$ plane are therefore equivalent, and they both can be expressed with the same principal stretches $\lambda_1 = 1/\lambda_3 = \lambda, \lambda_2 = 1$. The results presented here correspond to elongation in the X_2 direction.

The value of λ for each volume fraction is at least three times the elongation at failure observed experimentally [10]. Simulations

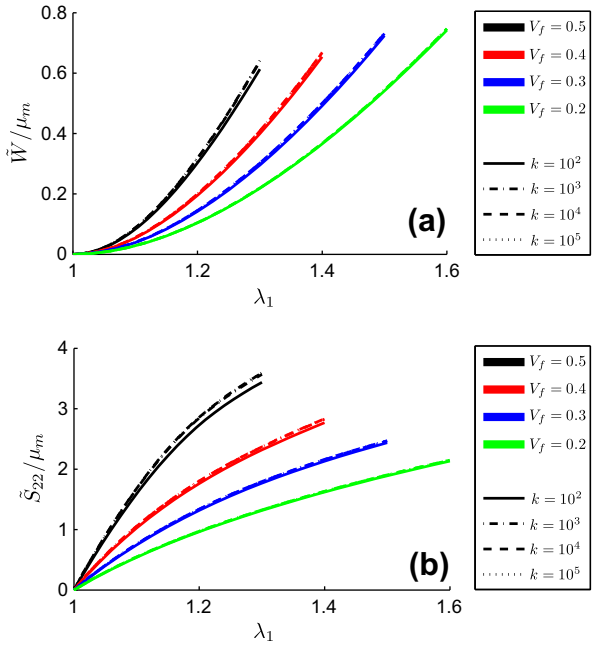

Fig. 4. Response of a composite with Neo-Hookean matrix and V_f fiber volume fraction to in-plane shear (shear in the $X_2 - X_3$ plane): (a) strain energy density normalized by the initial matrix shear stiffness vs. principal stretch and (b) nominal stress normalized by the initial matrix shear stiffness vs. principal stretch. The results for fiber–matrix stiffness ratios between $k = 10^3$ and $k = 10^5$ overlap into a single line.

considering different values of $k = \mu_f/\mu_m$ are shown in Fig. 4. The results overlap for the range of typical elastomers and reinforcing fibers ($k > 1000$), and even for $k = 100$ only small differences can be seen at high fiber volume fractions. The reason is that the high stiffness of the inclusions makes them behave as rigid bodies, and so μ_m is the only stiffness playing a role in the material. In the rest of this article, it is assumed that $k \geqslant 1000$, and the results are presented scaled by μ_m.

The numerical results are compared to the homogenization models in Fig. 5. The Hashin–Shtrikman bound underestimates the composite stiffness, and the difference increases with the fiber concentration, up to 30% when $V_f = 0.5$. The iterative homogenization provides a much closer agreement for low volume fractions, and even for $V_f = 0.5$ the error is of about only 15%. This suggests that polydispersity is inconsequential for small and moderate fiber concentrations.

The effect of the matrix behavior is shown in Fig. 6, where simulations with all three Ogden matrices are compared. As expected, the deviations increase with the fiber volume fraction, due to the higher strain concentrations between closely packed fibers.

The strain energy density of the composite normalized by the strain energy density of the corresponding matrix material subjected to the same macroscopic deformation is shown Fig. 7. Deviations from a constant value imply dependance on $\bar{I}_2$ or higher order terms of $\bar{I}_1$. These are much more prominent for models with an Ogden matrix.

Finally, the numerical model is also useful to study fields at the microscopic level. Fig. 8 shows how regions with high strain energy density tend to appear between closely packed fibers and aligned with the stretch direction, with maximum values of the local principal stretches well over ten times higher than the macroscopic applied loading.

4.2. Out-of-plane shear

In the case of the three-dimensional loadings only the strain energy density will be plotted. The effect of the Ogden matrices

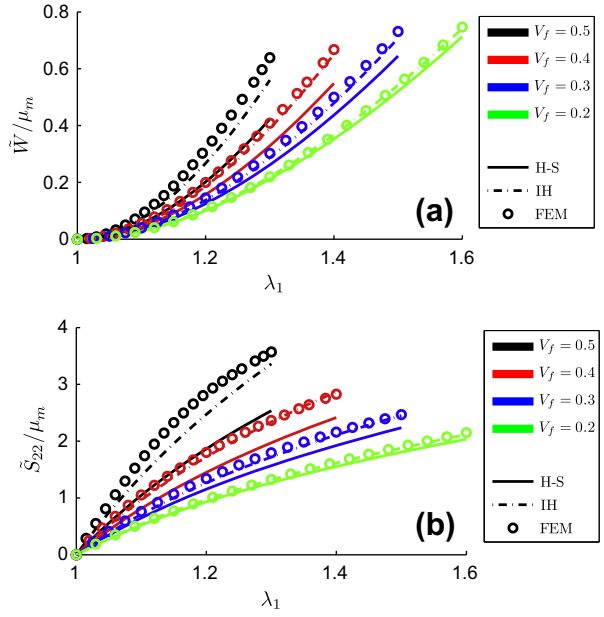

Fig. 5. Response of a composite with Neo-Hookean matrix and V_f fiber volume fraction to in-plane shear (shear in the $X_2 - X_3$ plane): (a) strain energy density normalized by the initial matrix shear stiffness vs. principal stretch and (b) nominal stress normalized by the initial matrix shear stiffness vs. principal stretch.

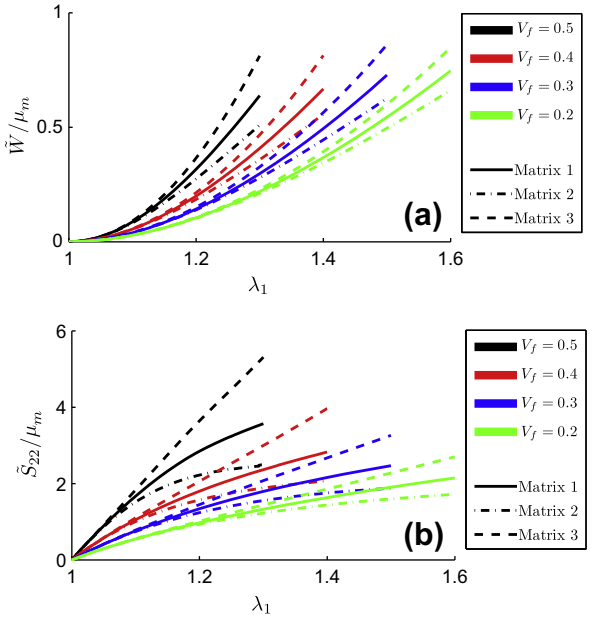

Fig. 6. Response of a composite with Ogden matrix and V_f fiber volume fraction to in-plane shear (shear in the $X_2 - X_3$ plane): (a) strain energy density normalized by the initial matrix shear stiffness vs. principal stretch and (b) nominal stress normalized by the initial matrix shear stiffness vs. principal stretch.

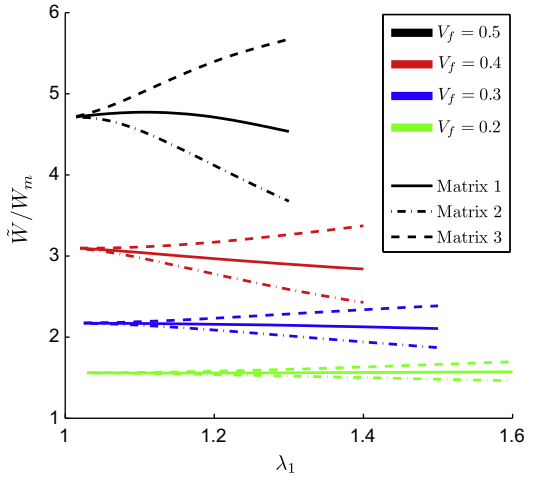

Fig. 7. Response of a composite with Ogden matrix and V_f fiber volume fraction to in-plane shear (shear in the $X_2 - X_3$ plane): strain energy density normalized by the strain energy density of the corresponding matrix material subjected to the same macroscopic deformation vs. principal stretch.

is basically the same as that shown in Fig. 6, and it is also omitted for conciseness.

The deformation gradient consists on shear in the $X_1 - X_3$ plane, which due to the condition $\bar{I}_4 = 1$ results in rotation of the fibers θ, see Fig. 9. Additionally, incompressibility results in a slight expansion in the X_2 and X_3 directions. A similar deformation state takes place during fiber microbuckling.

The corresponding macroscopic deformation gradient for a transversely isotropic solid is:

$$\bar{\mathbf{F}} = \begin{pmatrix} \cos(\theta) & 0 & 0 \\ 0 & 1/\sqrt{\cos(\theta)} & 0 \\ \sin(\theta) & 0 & 1/\sqrt{\cos(\theta)} \end{pmatrix} \tag{15}$$

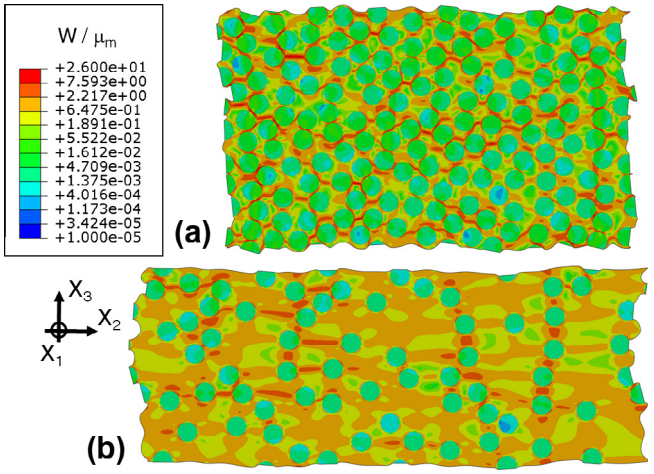

Fig. 8. Strain energy density of a composite with Neo-Hookean matrix under in-plane shear (shear in the $X_2 - X_3$ plane), normalized by the initial matrix shear stiffness (logarithmic scale): (a) $V_f = 0.5, \lambda_1 = 1.3$ and (b) $V_f = 0.2, \lambda_1 = 1.6$.

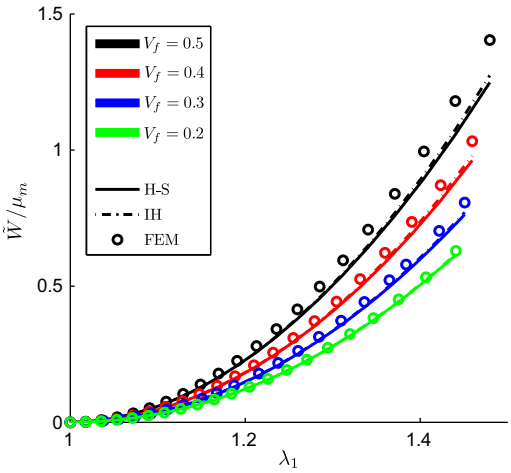

Fig. 10. Response of a composite with Neo-Hookean matrix and V_f fiber volume fraction to out-of-plane shear (shear in the $X_1 - X_3$ plane): strain energy density normalized by the initial matrix shear stiffness vs. principal stretch.

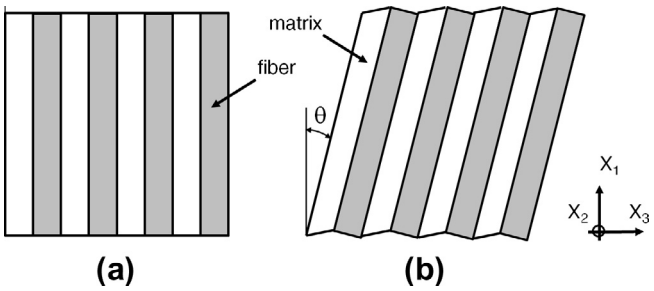

Fig. 9. Schematic of the response of a composite to out-of-plane shear (shear in the $X_1 - X_3$ plane): (a) undeformed configuration and (b) deformed configuration, showing that a microscopic level the deformation consists on rotation of the fibers and shear in the matrix.

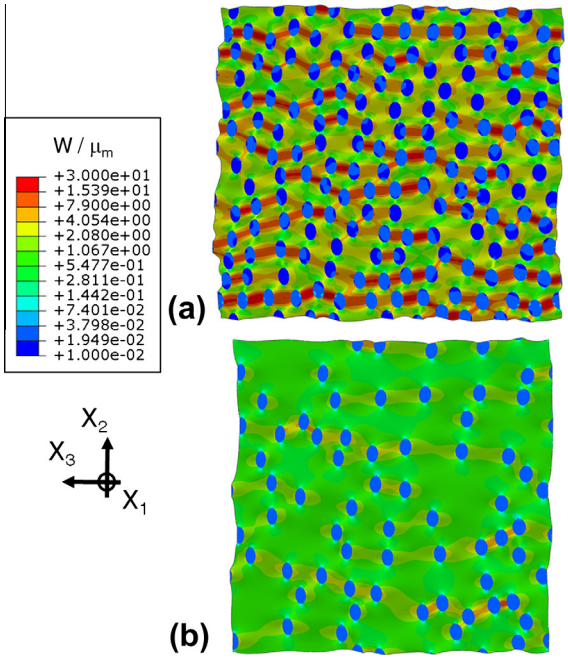

Fig. 11. Strain energy density of a composite with Neo-Hookean matrix under out-of-plane shear (shear in the $X_1 - X_3$ plane), normalized by the initial matrix shear stiffness (cross section, logarithmic scale): (a) $V_f = 0.5, \theta = \pi/4$ and (b) $V_f = 0.2, \theta = \pi/4$.

The simulations results deviate slightly from Eq. (15) due to the microstructure of the RVEs not being completely transversely isotropic, and so the values of $\tilde{\mathbf{F}}$ have been calculated from the displacement of the dummy nodes, $\mathbf{u}^i$ in Eq. (3). The applied shear is $\partial dx_1/\partial dX_1 = \partial dx_3/\partial dX_1 = \sqrt{2}/2$, corresponding to $\theta = \pi/4$, which is beyond the shear observed in the folding microbuckling of soft fiber composites when fiber failure takes place [12].

In this case the Hashin–Shtrikman lower bound and the iterative homogenization prediction are almost identical, and provide a good prediction of the numerical results, see Fig. 10. Only at high fiber concentrations the predictions underestimate the strain energy density, with 10% difference at $V_f = 0.5$.

The effect of the shear direction can also be observed in the micromechanics of the composite. In the case of out-of-plane shear the fibers rotate without changing their relative position, see Fig. 11. This results in a more homogeneous strain density field, which in turn leads to an overall softer response.

4.3. Comparison of in-plane and out-of-plane shear

The previous simulations have shown that the composite exhibits different behavior depending on the orientation of the applied shear. In order to better compare the results, the strain energy density of the composite normalized by the strain energy density of the matrix subjected to the same macroscopic deformation is plotted in Fig. 12 as a function of the $\bar{I}_1$ invariant. It is clear that the response depends on the direction of the applied shear, specially for high fiber volume fractions. Since the first three invariants are isotropic, and $\bar{I}_4 = 1$ throughout the simulations, the anisotropy must depend on the fifth invariant, $\bar{I}_5$. Additionally, the response to out-of-plane shear is very close to that of a Neo-Hookean material, with $\tilde{W}/W_m$ close to constant at all fiber volume fractions and values of $\bar{I}_1$, while for in-plane shear some dependance on $\bar{I}_2$ or higher order terms of $\bar{I}_2$ is observed at high strains.

Although the composite initial shear stiffness $\tilde{\mu}$ as a function of the fiber volume fraction and the loading direction can be inferred from Fig. 12, it is seen more clearly in Fig. 13, where it is compared with the homogenization predictions, $\tilde{\mu}_{HS}$ and $\tilde{\mu}_i$. The results show how starting from a common value for the dilute limit, the initial shear stiffness of both cases grow apart as the fiber concentration increases. The homogenization predictions are very close to the

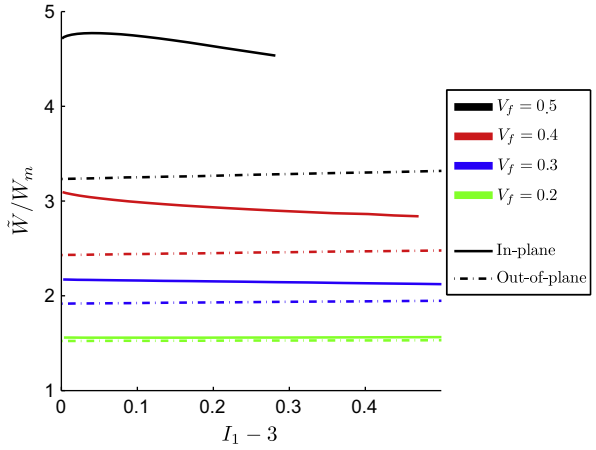

Fig. 12. Strain energy density of a composite with Neo-Hookean matrix and fiber volume fraction V_f under in-plane and out-of-plane shear, normalized by the strain energy density of the matrix subjected to the same macroscopic deformation vs. first invariant.

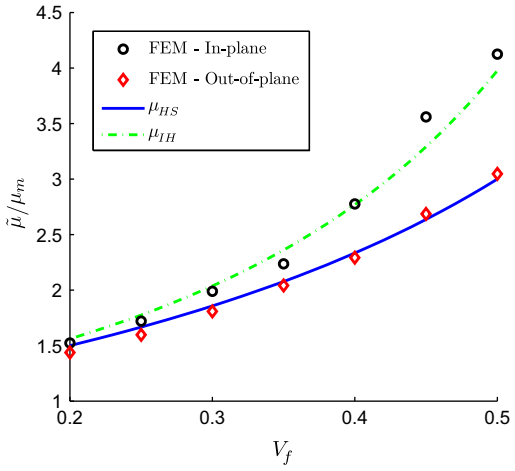

Fig. 13. Initial shear stiffness of a composite with Neo-Hookean matrix fiber volume fractions V_f under in-plane and out-of-plane shear loading, normalized by the matrix shear stiffness vs. fiber volume fraction.

corresponding numerical values; in order to accurately capture the behavior of the material, models needs to distinguish between both deformation modes through the dependance on $\bar{I}_5$.

4.4. Combined in-plane and out-of-plane shear

The dependance on the loading direction is further explored with simulations combining in-plane and out-of-plane shear. The imposed deformation is $\partial dx_3/\partial dX_2 = \delta_{23}$ and $\partial dx_3/\partial dX_1 = \delta_{13}$, plus the restraints $\bar{I}_3 = \bar{I}_4 = 1$. The corresponding average deformation gradient is:

$$\bar{\mathbf{F}} = \begin{pmatrix} (1-\delta_{13}^2)^{1/2} & 0 & 0 \\ 0 & (1-\delta_{13}^2)^{-1/4} & 0 \\ \delta_{13} & \delta_{23} & (1-\delta_{13}^2)^{-1/4} \end{pmatrix} \tag{16}$$

Defining the shear mixity as $\beta = \arctan(\delta_{13}/\delta_{23})$, in-plane and out-of-plane shear correspond to $\beta = 0$ and $\beta = \pi/2$, respectively. Numerical results for intermediate values, $\beta = \pi/6$ and $\beta = \pi/3$, are compared with the predictions of the iterative diluted homogenization scheme. The agreement is very close for concentrations up to $V_f = 0.4$, see Fig. 14. Even at $V_f = 0.5$ and $\beta = \pi/6$ the disagreement is below 10%.

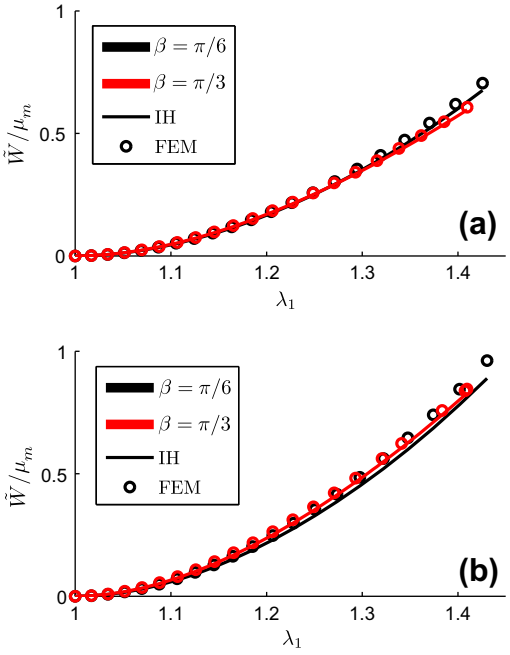

Fig. 14. Strain energy density of a composite with Neo-Hookean matrix and fiber volume fraction V_f under combined in-plane and out-of-plane shear (strain mixity β), normalized by the initial matrix shear stiffness vs. principal stretch: (a) $V_f = 0.4$ and (b) $V_f = 0.5$.

5. Discussion

The behavior of fiber-reinforced elastomers under three-dimensional loading has been studied through finite element models. The simulations use a set of two- and three-dimensional representative volume element with random fiber arrangement and periodic boundary conditions. The fibers are several orders of magnitude stiffer than the matrix, which is modeled as either a Neo-Hookean or Ogden hyperelastic material.

The simulations have focused on cases with no fiber stretching, $\bar{I}_4 = 1$. It has been found that the response to in-plane and out-of-plane shear is different, even at the linear regime, and that the difference increases with the fiber concentration. Since the first three invariants are isotropic, and the fourth invariant remains constant during the simulations, the anisotropy depends on the fifth invariant, $\bar{I}_5$. This deviation from a Neo-Hookean response for composites under shear is even more clear when the matrix is an Ogden hyperelastic solid with increased nonlinearity at high strains.

These results have been compared with two different homogenization based models. The shear response for laminated composites coincides with the Hashin–Shtrikman lower bound, and provides a very good prediction for the response to out-of-plane shear, but underestimates the in-plane shear stiffness. This can in turn be predicted with a new scheme using iterative dilute homogenization. A model combining both predictions with a linear dependance on $\bar{I}_5$ is able to capture both cases, as well as others in which both shear loadings are combined. Additional simulations, currently in progress, will be able to confirm this dependance, and determine if the small deviations observed at high fiber volume fractions can be attributed to higher order dependance on the strain invariants.

Acknowledgements

Support by the PSA Chair André Citroën is gratefully acknowledged. The author would also like to thank Prof. Oscar Lopez-Pamies (UIUC) for the results of the iterated dilute homogenization, and Dr. Kostas Danas (LMS, École Polytechnique) for useful discussions.

References

[1] Agoras M, Lopez-Pamies O, Ponte Castañeda P. A general hyperelastic model for incompressible fiber-reinforcedelastomers. J Mech Phys Solids 2009;57:268–86.
[2] Agoras M, Lopez-Pamies O, Ponte Castañeda P. Onset of macroscopic instabilities in fiber-reinforced elastomers at finite strain. J Mech Phys Solids 2009;57:1828–50.
[3] deBotton G. Transversely isotropic sequentially laminated composites in finite elasticity. J Mech Phys Solids 2005;53:1334–61.
[4] deBotton G, Hariton I, Socolsky E. Neo-hookean fiber-reinforced composites in finite elasticity. J Mech Phys Solids 2006;54:533–59.
[5] Francis WH, Lake MS, Schultz MR, Campbell D. Elastic memory composite microbuckling mechanics: closed-form model with empirical correlation. In: 48th AIAA/ASME/ASCE/AHS/ASC structures, structural dynamics, and materials conference. Honolulu, HI; 2007.
[6] Hill R. On constitutive macro-variables for heterogeneous solids at finite strain. Proc R Soc A 1972;326:131–47.
[7] Khisaeva Z, Ostoja-Starzewski M. On the size of rve in finite elasticity of random composites. J Elasticity 2006;85:153–73.
[8] Le Tallec P, Boussetta R, Lignon E. An enriched model of fiber-reinforced thin flexible structures with inplane buckling capabilities. Int J Numer Methods Eng 2012;91:872–95.
[9] Lignon E, Le Tallec P, Triantafyllidis N. Onset of failure in a fiber reinforced elastomer under constrained bending. Int J Solids Struct 2013;50:279–87.
[10] López Jiménez F, Pellegrino S. Constitutive modeling of fiber composites with a soft hyperelastic matrix. Int J Solids Struct 2012;49:635–47.
[11] López Jiménez F, Pellegrino S. Folding of fiber composites with a hyperelastic matrix. Int J Solids Struct 2012;49:395–407.
[12] López Jiménez F, Pellegrino S. Failure of carbon fibers at a crease in a fiber-reinforced silicone sheet. J Appl Mech 2013;80:353–60.
[13] Lopez-Pamies O. Private communication.
[14] Lopez-Pamies O. An exact result for the macroscopic response of particle-reinforced Neo-Hookean solids. J Appl Mech 2010:77.
[15] Lopez-Pamies O, Idiart MI. Fiber-reinforced hyperelastic solids: a realizable homogenization constitutive theory. J Eng Math 2010;68:57–83.
[16] Lopez-Pamies O, Ponte Castañeda P. On the overall behavior, microstructure evolution, and macroscopic stability in reinforced rubbers at large deformations: II – Application to cylindrical fibers. J Mech Phys Solids 2006;54:831–63.
[17] Michel J, Lopez-Pamies O, Ponte Castañeda P, Triantafyllidis N. Microscopic and macroscopic instabilities in finitely strained porous elastomers. J Mech Phys Solids 2007;55:900–38.
[18] Moraleda J, Segurado J, Llorca J. Finite deformation of incompressible fiber-reinforced elastomers: a computational micromechanics approach. J Mech Phys Solids 2009;57:1596–613.
[19] Ogden RW. Large deformation isotropic elasticity – on the correlation of theory and experiment for incompressible rubberlike solids. Proc R Soc London 1972;326:565–84.
[20] Pandolfi A, Holzapfel GA. Three-dimensional modeling and computational analysis of the human cornea considering distributed collagen fibril orientations. J Biomech Eng 2008:130.
[21] Perotti L, Deiterding R, Inaba K, Shepherd J, Ortiz M. Elastic response of water-filled fiber composite tubes under shock wave loading. Int J Solids Struct 2013;50:473–86.
[22] Rintoul M, Torquato S. Reconstruction of the structure of dispersions. J Colloid Interface Sci 1997;186:467–76.
[23] Rudykh S, deBotton G. Instabilities of hyperelastic fiber composites: micromechanical versus numerical analyses. J Elasticity 2012;106:123–47.
[24] Spencer AJM. Constitutive theory of strongly anisotropic solids. In: for Mechanical Sciences, I.C., editor. Continuum theory of the mechanics of fibre-reinforced composites; 1972.
[25] Tanemura M. On random complete packing by disks. Ann Inst Stat Math 1979;31:351–65.